Dynamic Exchange During Triplet Transport in Nanocrystalline TIPS-Pentacene Films

Christopher Grieco,[†] Grayson S. Doucette,[‡] Ryan D. Pensack,[§] Marcia M. Payne,[||] Adam Rimshaw,[†] Gregory D. Scholes,[§] John E. Anthony,*[,||] and John B. Asbury*[,†,‡]

[†]Department of Chemistry, The Pennsylvania State University, University Park, Pennsylvania 16802, United States
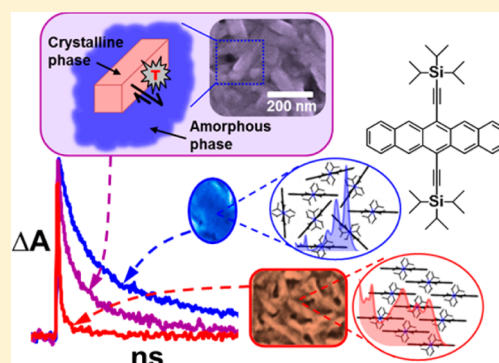
[‡]Intercollege Materials Science and Engineering Program, The Pennsylvania State University, University Park, Pennsylvania 16802, United States

[§]Department of Chemistry, Princeton University, Princeton, New Jersey 08544, United States

[||]Department of Chemistry, University of Kentucky, Lexington, Kentucky 40506, United States

S *Supporting Information*

ABSTRACT: The multiplication of excitons in organic semiconductors via singlet fission offers the potential for photovoltaic cells that exceed the Shockley−Quiesser limit for single-junction devices. To fully utilize the potential of singlet fission sensitizers in devices, it is necessary to understand and control the diffusion of the resultant triplet excitons. In this work, a new processing method is reported to systematically tune the intermolecular order and crystalline structure in films of a model singlet fission chromophore, 6,13-bis(triisopropylsilylethynyl) pentacene (TIPS-Pn), without the need for chemical modifications. A combination of transient absorption spectroscopy and quantitative materials characterization enabled a detailed examination of the distance- and time-dependence of triplet exciton diffusion following singlet fission in these nanocrystalline TIPS-Pn films. Triplet−triplet annihilation rate constants were found to be representative of the weighted average of crystalline and amorphous phases in TIPS-Pn films comprising a mixture of phases. Adopting a diffusion model used to describe triplet−triplet annihilation, the triplet diffusion lengths for nanocrystalline and amorphous films of TIPS-Pn were estimated to be ∼75 and ∼14 nm, respectively. Importantly, the presence of even a small fraction (<10%) of the amorphous phase in the TIPS-Pn films greatly decreased the ultimate triplet diffusion length, suggesting that pure crystalline materials may be essential to efficiently harvest multiplied triplets even when singlet fission occurs on ultrafast time scales.

■ INTRODUCTION

Singlet fission is an exciton multiplication mechanism observed in a variety of small organic molecular systems[1] that promises to improve current solar cell technology by boosting device photoconversion efficiencies beyond the Shockley−Queisser Limit.[2] In fact, singlet fission quantum efficiencies as high as 200% have been demonstrated.[3,4] Use of singlet fission sensitizers to enhance the efficiency of functional devices requires energy or electron transfer from the multiplied excitons to other elements of the optoelectronic device.[5−8] Therefore, efficient singlet fission is a necessary but insufficient condition for using singlet fission sensitizers in practical applications. The dynamics of the triplet excitons following the singlet fission process must also be considered.[9]

Efficient energy or electron transfer from triplet excitons to other elements of an optoelectronic device require that the triplet excitons have adequate transport properties resulting from long lifetimes and high diffusion constants.[10−13] The diffusion of triplet excitons over tens to hundreds of nanometers in highly crystalline organic films and over micrometers in ultrahigh purity single crystals have been

characterized by device studies,[5−8] photocurrent modulation,[10] and by ultrafast microscopy.[11−13] However, as new singlet fission sensitizers are explored,[14−17] it is likely that not all singlet fission materials will form highly ordered films,[18] especially as polymers are being targeted[19−22] for their superior processing flexibility. For example, exciton diffusion from disordered regions to "dimer" sites in nanocrystalline films has been observed from ultrafast measurements of singlet fission.[15,23] These and other papers[24−29] reported the sensitivity of the rate and yield of singlet fission on the intermolecular interactions and crystal structures of the materials. While the majority of this work has focused on factors that affect the rates of singlet fission, there remains a need to understand the transport of triplet excitons formed by singlet fission and how this is influenced by the nanocrystalline morphology that is characteristic of thin films of organic optoelectronic materials.

In this work, we report a new solvent annealing method to systematically tune the molecular-level packing and morphol-

ogy in thin films of a model singlet fission chromophore, 6,13-bis(triisopropylsilylethynyl)pentacene (TIPS-Pn, Figure 1a).
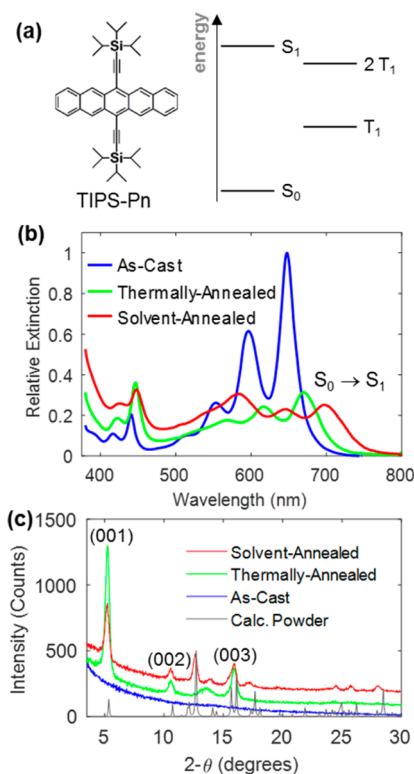

Figure 1. (a) Structure of TIPS-Pn and diagram of initial and final states relevant to singlet fission. (b) Absorbance spectra of distinct polymorphs of TIPS-Pn present in films annealed under various conditions. The spectra were used as basis spectra for the 3-state spectral model used to quantify the composition of partially annealed films that were examined in this study. (c) Grazing-incidence X-ray diffraction patterns measured for TIPS-Pn films on sapphire substrates annealed under various conditions.

This method permitted us to systematically vary the strength of molecular interactions and the polymorphs present in TIPS-Pn films without the need to modify the chemical structure as has been used in the past to vary similar properties among singlet fission chromophores.[26,29−31] We used the ability to tune the molecular-level packing and morphology in TIPS-Pn films to systematically investigate the diffusion of triplet excitons between amorphous and nanocrystalline domains.

We found that the rates of singlet fission measured in TIPS-Pn films depended on their molecular-level packing and crystallinity similar to prior observations.[15,23−29] However, the most dramatic changes were observed in the diffusion-controlled triplet−triplet annihilation processes, which suggested that the triplet transport characteristics depended sensitively on molecular-level order and film morphology. Quantitative structural and optical characterization revealed that triplet excitons underwent annihilation processes that reflected the average properties of the films consisting of nanocrystalline domains mixed with amorphous phases of TIPS-Pn molecules. Triplet excitons were able to diffuse over distances sufficiently large that their annihilation kinetics were determined by the mole fractions of the crystalline and amorphous phases in the nanocrystalline TIPS-Pn films. Adopting a diffusion model used to describe triplet−triplet annihilation,[32,33] the triplet diffusion lengths were estimated for

nanocrystalline films containing varying mole fractions of the amorphous versus crystalline phases of TIPS-Pn. The results of this study reveal that triplet excitons are able to undergo dynamic exchange across phase boundaries between amorphous and crystalline domains of TIPS-Pn. Furthermore, the study reveals that even small amounts of an amorphous phase in singlet fission sensitizer films can significantly decrease the ultimate triplet diffusion length, suggesting that highly crystalline materials may be needed to efficiently harvest the multiplied triplet excitons even when the singlet fission can occur on ultrafast time scales.

■ RESULTS AND DISCUSSION

Tuning Molecular-Level Packing and Crystallinity in TIPS-Pn Films. TIPS-Pn is known to form several polymorphs depending on the conditions of film or crystal formation.[34−36] The 2D-brickwork crystal structure is commonly accessed by deposition of TIPS-Pn films.[26,34,37,38] Diao et al.[34] recently used solution-shearing of films to isolate other TIPS-Pn polymorphs and showed using differential scanning calorimetry and X-ray diffractometry that these polymorphs interconvert at characteristic temperatures. However, the solution-shearing approach produced extremely thin films that are challenging to study using ultrafast spectroscopy. In an effort to explore the impact of molecular-level interactions and film morphology on the dynamics of the triplet excitons that result from singlet fission, we developed methods to spin-cast disordered films of TIPS-Pn, convert these disordered films to particular polymorphs, and systematically tune the morphology of the TIPS-Pn films via control of deposition and annealing conditions.

We considered that selection of appropriate solute−solvent interactions in combination with a volatile solvent would result in disordered TIPS-Pn films containing weakly coupled chromophores. Furthermore, we observed that thermal annealing[39] at a moderate temperature and slow solvent annealing with an appropriate solvent enabled us to controllably access two distinct polymorphs in TIPS-Pn films. Figure 1b depicts visible absorption spectra of TIPS-Pn films spin-cast from dichloromethane without subsequent annealing ("as-cast" spectrum), with subsequent thermal annealing at 100 °C for 1 min ("thermally annealed" spectrum), and with slow solvent annealing in 2-propanol vapor for 60 min ("solvent-annealed" spectrum). The films used to measure the spectra were selected to have the same thicknesses with a precision of ±2% as characterized by their initial absorption spectra prior to thermal- or solvent-annealing. Therefore, the amplitudes of the absorption spectra represent the relative extinction coefficients of the films. The absorption spectra of the TIPS-Pn films exhibit distinct shapes that are characteristic of each polymorph in the respective films because excitonic effects that determine the shapes of each absorption spectrum depend sensitively on molecular-level packing.[29]

We characterized the TIPS-Pn films using grazing-incidence X-ray diffraction (GIXRD) in an effort to gain further insight about the molecular-level interactions present in each film. Figure 1c represents GIXRD patterns measured in the as-cast, thermally annealed, and solvent-annealed films. Cu Kα radiation was used to collect the diffraction patterns at a 1° angle of incidence. The calculated powder diffraction pattern is shown in gray for reference. The diffraction patterns have been offset for clarity of presentation. The as-cast film exhibited no discernible diffraction peaks indicating a lack of significant long-range order in the film. In contrast, a diffraction pattern is

clearly observed in the solvent-annealed film that closely matches patterns reported in TIPS-Pn films in which the molecules adopt the 2D-brickwork crystal structure.[26,34,37,38] To ensure the diffraction patterns were representative of the films and not biased due to epitaxial growth on the single crystal sapphire substrates, we performed the GIXRD measurement using multiple sample rotations (Section S5). We did not observe preferential orientations of the crystallites in the lateral plane (parallel to the substrate surface).

The thermally annealed film exhibits (001), (002) and (003) reflections similar to the solvent-annealed film suggesting that the crystal planes in the crystallographic c-direction (separated by the triisopropylsilylethynyl side groups in the molecules) are similar in both films. However, a broad peak appears around 13.5° $2-\theta$ for the thermally annealed film that is missing in the solvent annealed film, indicating differences in molecular packing along the other crystallographic directions. Changes in these diffraction peaks have been associated with formation of different polymorphs of TIPS-Pn.[34,36] In particular, the Form-II brickwork structure identified by Diao et al.[34] most closely resembles the structure present in our thermally annealed films on the basis of these diffraction peaks in conjunction with the unique locations of the vibronic peaks in the absorption spectrum of the film. We note that the different absorption spectra of the thermally versus solvent-annealed films (Figure 1b) are consistent with different molecular packing structures *within* the (001) plane of the crystals because this plane includes pi-pi stacking, which strongly affects the electronic interactions between molecules and therefore the absorption spectra of the films. We will henceforth refer to the phase accessed by thermal annealing as the Form-II brickwork structure in the following discussion. To our knowledge, this is the first report of this type of TIPS-Pn polymorph isolated in a thick (∼100 nm) film deposited via spin-coating.

We desired to more finely tune the distribution of polymorphs present in TIPS-Pn films using our gentle solvent-annealing method in an effort to systematically explore how molecular packing arrangements and nanoscale morphologies in the films affect the dynamics of triplet excitons formed by singlet fission. Figure 2a represents visible absorption spectra measured in a series of TIPS-Pn films that were annealed in 2-propanol vapor for different periods of time. The "as-cast" and the "1 hr" spectra were reproduced from the "as-cast" and "solvent-annealed" spectra in Figure 1b, respectively. The absorption spectrum of the as-cast TIPS-Pn film closely matched the spectrum of isolated TIPS-Pn molecules measured in dilute toluene solution. In particular, the "vibronic fingerprint" of the as-cast film was very similar to that of the dilute solution (compare the dotted black and solid blue traces in Figure 2a), indicating that the electronic interactions between chromophores were weak. As a result, there was not a gross redistribution of the vibronic bands in the transition between S_0 and S_1 in the 600−700 nm range in the as-cast film that are typically observed in polycrystalline films.[29] We concluded therefore that TIPS-Pn molecules in the as-cast film were weakly coupled similar to "Type I nanoparticles" recently reported by Pensack et al.[29]

Using 2-propanol as the annealing solvent enabled us to precisely control the extent of annealing by varying the duration of exposure to the solvent vapor as captured by the series of absorption spectra appearing in Figure 2a. The spectra indicated film evolution from weakly coupled (thick blue
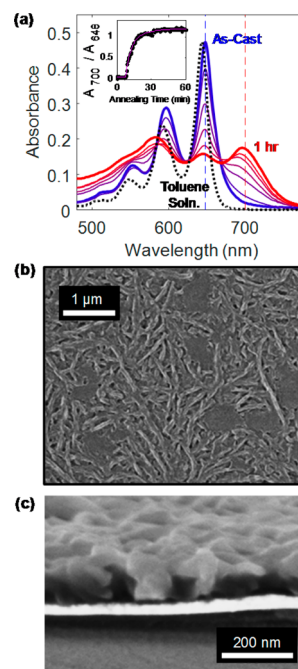

Figure 2. (a) Evolution of the absorbance spectrum of TIPS-Pn films from as-cast to fully annealed. The dashed black spectrum represents a dilute TIPS-Pn/Toluene solution. The inset shows the annealing kinetics, represented as the absorbance ratio of A_{700}/A_{648}. (b) SEM image of a partially annealed TIPS-Pn film showing crystalline and amorphous domains. (c) Cross-sectional SEM image of a partially solvent-annealed TIPS-Pn film on a Au coated substrate showing the growth of <100 nm crystallites.

trace) to the highly ordered 2D-brickwork phase that commonly forms in TIPS-Pn films.[26,34,37,38]

To facilitate subsequent discussion, we quantified the extent of annealing by calculating the ratio of absorbance of each film at the 0−0 transition of crystallized TIPS-Pn at 700 nm versus the 0−0 peak of disordered molecules at 648 nm (A_{700}/A_{648}). These wavelengths are noted by the red and blue dashed vertical lines in Figure 2a. This metric will be used in the subsequent discussion to refer to TIPS-Pn films annealed to various extents. The inset in Figure 2a represents the variation of this metric versus solvent-annealing time in minutes, empirically fit using a biexponential growth model. The A_{700}/A_{648} ratio reaches an asymptotic limit after 60 min of continuous solvent-annealing. We therefore considered films annealed for this time duration as fully solvent-annealed and refer to them as such in the following discussion. More information about the annealing method is described in the Supporting Information (Section S3).

A scanning electron microscopy (SEM) image of a partially solvent-annealed TIPS-Pn film on gold is represented in Figure 2b. The image of the film was captured at an early stage of the annealing process and revealed the formation of TIPS-Pn crystals that broke out from the surface of the originally amorphous (smooth) film. Furthermore, smooth regions remain in the film that were eliminated upon continued annealing, indicating that the partially annealed film consisted of a mixture of crystalline and amorphous domains. A cross sectional SEM image of a partially solvent-annealed TIPS-Pn film made on a gold-coated glass coverslip confirms the formation of features of <100 nm dimension (Figure 2c). For reference, SEM images over larger areas and at different stages

of annealing are provided in Section S12. The GIXRD patterns presented in Section S7 demonstrate that the molecular packing in the crystalline regions of the partially solvent-annealed films was similar to that found in the fully solvent-annealed films.

Because the visible absorption spectra of TIPS-Pn were sensitive to the molecular-level packing of the molecules (see Figure 1b), we used the evolution of the absorption spectra versus solvent-annealing time to quantify the amorphous and crystalline phases in each film. The SEM image represented in Figure 2b suggested that the composition of the partially annealed films could be described by a mixture of crystalline and amorphous phases of varying proportion. Therefore, we constructed a model to fit the visible absorption spectra of the partially annealed films consisting of a linear combination of basis spectra corresponding to the amorphous and crystalline phases of TIPS-Pn. We found it necessary to include three basis spectra in the model corresponding to the amorphous (as-cast), Form-II brickwork (thermally annealed), and 2D-brickwork (solvent-annealed) phases of TIPS-Pn (See Figure 1b) to adequately describe the visible absorption spectra. The three basis spectra are reproduced in Figure 3a along with the visible
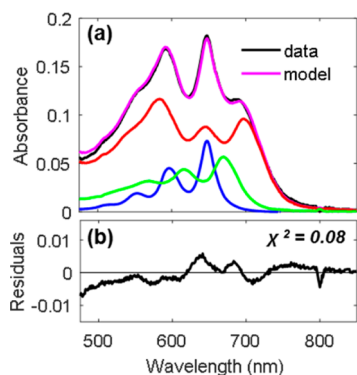

Figure 3. (a) Result of spectral decomposition of the A_{700}/A_{648} $r = 0.6$ film using the 3-state model including the spectra for the as-cast (blue), thermally annealed (green), and a solvent-annealed (red) films as the basis spectra. (b) Residuals calculated from the difference between the data and the spectrum from the 3-state model showing the fidelity of the fit.

absorption spectrum of a partially annealed film with an absorption ratio $A_{700}/A_{648} = 0.6$. Overlaid on the absorption spectrum of the partially annealed film is the best fit spectrum calculated using eq 1, where $A_{AC}(\lambda)$, $A_{TA}(\lambda)$ and $A_{SA}(\lambda)$ are the basis spectra corresponding to the absorption spectra of the as-cast, thermally annealed and solvent-annealed TIPS-Pn films, respectively.

$$f(\lambda) = N[w_{AC}A_{AC}(\lambda) + w_{TA}A_{TA}(\lambda) + w_{SA}A_{SA}(\lambda)] \quad (1)$$

$$w_{AC} + w_{TA} + w_{SA} = 1$$

The weighting factors w_i for each phase were constrained to a sum of unity to satisfy the physical constraint in the model that all TIPS-Pn molecules in the films exist in one of these three phases.

Because the basis spectra were already scaled by the relative absorption coefficients of their respective phases, the weighting factors represented the mole fractions of TIPS-Pn molecules in each phase in the partially solvent-annealed films. Figure 3b displays the residual spectrum obtained by subtracting the best

fit from the three-state model from the visible absorption spectrum of the partially annealed film. Note the more than order of magnitude difference in the amplitude scales of the absorbance and residual spectrum plots. The residual spectrum captured the fidelity of the fit. We demonstrate in Section S8 the necessity of including the Form-II brickwork phase in the linear combination to properly describe the absorption spectra of the partially solvent-annealed films. In all cases a simpler two-phase model (amorphous and 2D-brickwork) did not adequately describe the visible absorption spectra of the TIPS-Pn films. We note that there may be more than three packing arrangements present in solvent-annealed films such as those discovered in solution-sheared films.[34] In that work, Diao and co-workers related variations in the molecular packing present in different TIPS-Pn crystal polymorphs to changes in the vibronic peak positions of their absorbance spectra. We included the Form-II brickwork structure in our model because the residuals of the fit using the 2-state model (Figure S9b) contain features that qualitatively match the vibronic peak positions in this polymorph. This suggests that although there may be a variety of packing structures present in the solvent-annealed films, the Form-II brickwork provides an adequate description of the third component needed to describe the data.

Because we sought to investigate how the dynamics of multiplied triplet excitons resulting from singlet fission depend on molecular-level packing and morphology, we used the three-phase model to quantify the mole fractions of TIPS-Pn molecules in the amorphous, Form-II brickwork and 2D-brickwork phases in the partially solvent-annealed films. Figure 4 depicts the results of fitting the absorption spectra of TIPS-Pn
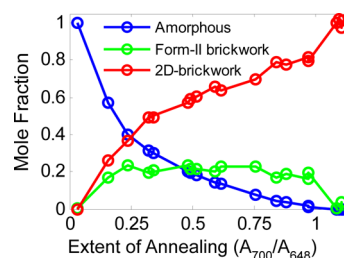

Figure 4. Results of the spectral decomposition using the 3-state model for films with a variety of extents of annealing. Each film was exposed to 2-propanol vapor for different annealing times ranging from minutes to an hour. The extent of annealing is represented as the ratio of the absorbance at 700 to 648 nm. The y-axis represents the mole fractions determined for each type of packing arrangement: Amorphous (blue), Form-II brickwork (green), and 2D-brickwork (red).

films annealed to varying extents using the three-phase model. Examples of individual absorbance spectra with their overlaid best fit spectra appear in Section S8. The mole fractions of each phase present in the films are arranged according to their corresponding ratio of absorption at 700 nm versus 648 nm. The analysis using the three-phase model revealed a monotonic decrease of the disordered population, a monotonic increase of the 2D-brickwork population, and a growth and decay of the Form-II brickwork population of TIPS-Pn molecules with continued solvent-annealing.

Finally, to quantify the crystallite sizes among the TIPS-Pn films solvent-annealed to varying extents, we measured 2D-diffraction patterns of the films at strategic points along the solvent-annealing process. We rocked the films over the (001)

peak appearing in the X-ray diffraction pattern around 5.4° $2-\theta$, which enabled us to quantify differences in the crystal packing along the c-direction in the TIPS-Pentacene crystallites without biasing particular crystallite orientations. The integrated (001) diffraction peaks for films annealed to varying extents are presented in Figure 5. As observed in the GIXRD
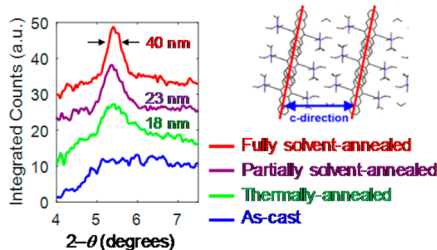

Figure 5. Integrated 2D-XRD patterns obtained by rocking over the (001) reflection peak for TIPS-Pentacene films solvent-annealed for different amounts of time. The fully solvent-annealed film exhibits the narrowest diffraction peak width, while the diffraction peak of the partially solvent-annealed film ($A_{700}/A_{648} = 0.7$) is broader. The diffraction pattern for a thermally annealed film (Type-II brickwork) is shown for reference as the green trace. The average crystallize sizes determined using Scherrer analysis are indicated.

measurements (Figure 1c), the amorphous (as-cast) films did not exhibit a peak, confirming a lack of long-range molecular-order among the TIPS-Pn molecules. For the fully solvent-annealed film, the integrated rocking scan resulted in a peak center around ~5.4° $2-\theta$ with the smallest full-width at half-maximum, corresponding to the largest average crystallite size among the set of films. An integrated rocking curve of a thermally annealed film also appears in Figure 5 for comparison. Both the Form-II and 2D-brickwork structures of TIPS-Pn have similar (001) peak positions (see Figure 1c). However, the increased breadth of the (001) peak of the thermally annealed film indicated that the crystallites in this film were smaller than crystallites found in the fully solvent-annealed film. An integrated rocking curve of the (001) peak of a partially solvent-annealed film with A_{700}/A_{648} ratio = 0.7 was also measured and is compared to the other films, indicating that the crystallites in this film were intermediate in size between the fully solvent-annealed and the thermally annealed films.

We fit the widths of the (001) peaks of the films, corrected for the finite angular resolution of the diffractometer, and used Scherrer analysis to estimate the average crystallite sizes in the partially and solvent-annealed films. From this analysis, we obtained average crystallite sizes of 23 ± 3 nm and 40 ± 10 nm in the partially and fully solvent-annealed films, respectively, assuming a shape factor of 0.96 ± 0.09,[40] where the confidence limits were obtained by propagation of uncertainties in the fits and shape factor through the calculation as detailed in Section S13. Similarly, the thermally annealed (Form-II brickwork) film was determined to have an average crystallize size of 18 ± 2 nm. These crystallite sizes obtained from Scherrer analysis are qualitatively consistent with the ~50 nm wide features observed in the SEM images of TIPS-Pn films (see Figure 2).

Influence of Intermolecular Order on Triplet Transport and Decay. In the previous section, we described our efforts to control molecular-level packing and morphology in TIPS-Pn films through novel materials processing methods. Having characterized molecular-level and long-range order as a function of annealing conditions, we turned to investigate the transport and decay of triplet excitons resulting from singlet fission and how these properties depended on molecular-level and long-range order in the films. We first verified that singlet fission occurred on ultrafast time scales in our partially solvent-annealed TIPS-Pn films to show that the triplet excitons examined in the subsequent triplet—triplet annihilation study were formed principally from singlet fission rather than by intersystem crossing.

Figure 6a depicts nanosecond transient absorption spectra of TIPS-Pn films solvent annealed to various extents. The spectra
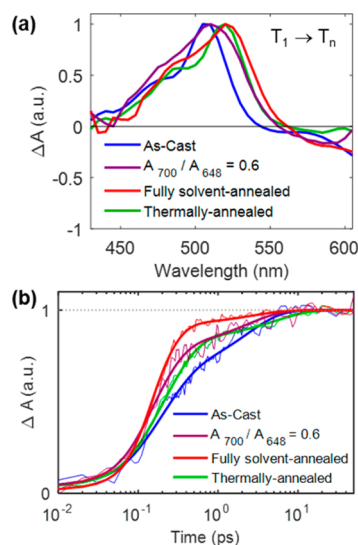

Figure 6. (a) Triplet photoinduced absorbance spectra ($T_1 \rightarrow T_n$) in the visible spectral region measured in TIPS-Pn films solvent-annealed to varying extents and thermally annealed. (b) Comparison of the triplet population growth kinetics measured in the TIPS-Pn films at the peaks of the $T_1 \rightarrow T_n$ transitions demonstrating that singlet fission occurs in all films on ultrafast time scales as expected.

of the as-cast, partially annealed ($A_{700}/A_{648} = 0.6$), fully solvent-annealed and thermally annealed films were measured 10 ns after excitation of the films at 649 nm and 30 μJ/cm^2 absorbed energy density. As seen in Figure 1b, 649 nm excitation corresponded to the $S_0 \rightarrow S_1$ electronic transition for all the films. The resulting transient absorption of TIPS-Pn probed in the visible spectral region around 525 nm has been assigned to a $T_1 \rightarrow T_n$ absorption that may also contain contributions from higher-lying triplet states.[41,42] The triplet state photoinduced absorption band exhibited a redshift in the fully annealed films consistent with an increased average intermolecular interaction between TIPS-Pn molecules.

Triplet formation kinetics as a result of singlet fission were measured on the femtosecond to picosecond time scale in the films at the maximum of the triplet absorptions determined from the $T_1 \rightarrow T_n$ spectra. The kinetics traces represented in Figure 6b were measured following photoexcitation at 655 nm and 20 μJ/cm^2 absorbed energy density. Across all extents of annealing, singlet fission was complete within the first 20 ps, which is characteristic of pentacene derivatives. The singlet fission kinetics in all films were well-described by the sum of two exponential growth functions.[29,43] The results of the fits are summarized in Table 1.

The double exponential growth model was convoluted with a Gaussian representing the instrument response function to

Table 1. Fit Results for the Ultrafast Triplet State Absorption Kinetics

sample name	$a_1{}^a$	$T_1{}^b$ (ps)	$a_2{}^a$	$T_2{}^b$ (ps)	$\langle T \rangle^c$ (ps)
as-cast	0.64	0.19	0.36	2.26	0.93
$A_{700}/A_{648} = 0.6$	0.79	0.14	0.21	2.30	0.59
fully solvent-annealed	0.92	0.11	0.08	2.60	0.32
thermally annealed	0.84	0.21	0.16	5.10	1.00

$^a a_1$ and a_2 are amplitude factors for the fast and slow exponential growth functions, respectively. $^b T_1$ and T_2 are the time constants for the fast and slow exponential growth functions, respectively. $^c \langle T \rangle$ is the weighted average time constant.

generate the fits presented in Figure 6b. Our time resolution was estimated to be 100 fs, which was the Gaussian full-width-at-half-maximum that best fit the kinetic rise in the data across the entire series. Furthermore, the observation of fast triplet formation dynamics that depend on the strength of intermolecular interactions and energetics in the films is consistent with results of prior investigations.[15,23−29] We therefore concluded that singlet fission was the principal origin of triplet excitons present in the TIPS-Pn films reported here regardless of their extent of annealing.

Having established that singlet fission occurs in our TIPS-Pn films with tunable morphology and packing arrangements, we examined the effect these material properties had on the transport and decay of the resulting multiplied triplet excitons. We chose to examine triplet transport in the TIPS-Pn films using the triplet−triplet annihilation method[7,33,44] because this approach enabled us to estimate triplet diffusion lengths directly from the triplet decay kinetics.

We recall that triplet−triplet annihilation is a diffusion-controlled bimolecular process that is governed by the ability of triplet excitons to transfer from molecule to molecule. The mechanism of triplet transfer includes a spin-forbidden de-excitation step, and so orbital-overlap-dependent electronic coupling mediates this process.[45] As a consequence, the rate of this transport process should depend sensitively on the types of intermolecular orbital overlap in the TIPS-Pn films.

We measured the kinetics of triplet decay on the nanosecond to microsecond time scale in our solvent-annealed films by probing at the peak of the corresponding $T_1 \rightarrow T_n$ transition (Figure 6a) following excitation at 649 nm. The triplet exciton decay kinetics presented in Figure 7a were measured following excitation with an absorbed energy density of ~20 μJ/cm^2. We defined the mole fraction of the ordered phases ϕ as the sum of the mole fractions of the Form-II brickwork and 2D-brickwork phases determined from analysis of the visible absorption spectra of each film as indicated in Figure 4. In Figure 7a, we labeled the triplet decay kinetics according to the total mole fraction of the ordered phases ϕ in each film. Henceforth, we will refer to partially solvent-annealed films by their mole fraction ϕ rather than by their A_{700}/A_{648} nm ratios because the mole fraction conveys more physical insight about the molecular-level interactions and nanoscale morphologies of the films. The relationship between these two metrics is captured in the phase composition analysis depicted in Figure 4.

We used a diffusion-dominated triplet−triplet annihilation model[7,33,44] to describe the triplet decay kinetics represented in Figure 7a. The model is characterized by the rate equation:
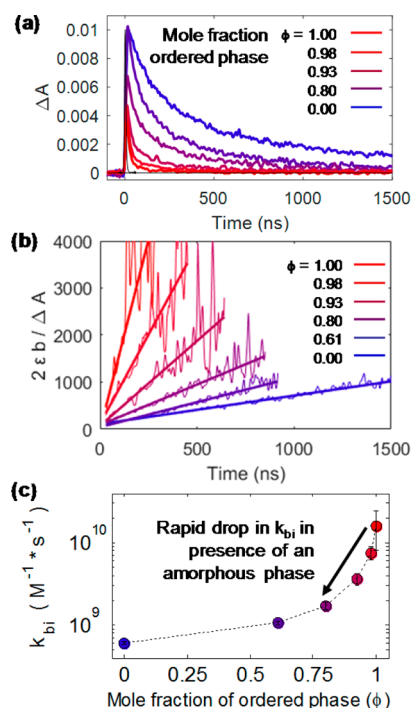
Figure 7. (a) Nanosecond decays of the triplet PIA for TIPS-Pn films solvent annealed for various durations. The traces are labeled by the mole fraction ϕ of total ordered phase (Form-II brickwork + 2D-brickwork). (b) Plot of $2\varepsilon b/\Delta A$ versus time, highlighting the bimolecular decay behavior of the triplets. The lines are linear fits to the data used to determine the bimolecular rate constants presented in (c). Note that the data have been corrected for differences in relative extinction coefficients among the films. (c) Relationship between bimolecular rate constants and the mole fractions of the ordered phases. Note the logarithmic scale. Note also that the inclusion of even small amounts of the amorphous phase in the films caused an order of magnitude decrease in triplet diffusivity.

$$\frac{d[T]}{dt} = -\frac{[T]}{\tau} - \frac{1}{2}k_{bi}[T]^2 \tag{2}$$

where $[T]$ is the triplet concentration, τ is the natural (unimolecular) triplet lifetime, k_{bi} is the second-order decay constant (bimolecular) describing triplet−triplet annihilation, and t is time. The prefactor $1/2$ in the second-order term is included because triplet−triplet annihilation typically does not result in elimination of both excited states. In the case of TIPS-Pn, triplet−triplet annihilation is believed to form one highly excited T_n state from two T_1 states because reformation of the S_1 state via triplet fusion is endergonic.[46] When the triplet concentration is sufficiently high (especially at short time delays and at moderate excitation densities) and when $1/\tau \ll k_{bi}[T]$, the second-order term dominates, allowing us to neglect the first term in eq 2. We demonstrated in Section S9 the validity of this assumption under the experimental conditions reported here. The solution of this simplified rate equation is

$$\frac{1}{[T]} = \frac{1}{[T_0]} + \frac{1}{2}k_{bi}t \tag{3}$$

which predicts that the inverse of the time-dependent triplet population should depend linearly on time with a slope equal to the $1/2$ multiplied by the second-order decay constant k_{bi}. Because the transient absorption signal measured at the peak of the $T_1 \rightarrow T_n$ transition was proportional to the concentration of

triplet excitons $[T]$ multiplied by the molar absorption coefficient and path length εb, the model shows that a plot of the inverse transient absorption signal $1/\Delta A$ versus t should exhibit linear behavior with the form

$$\frac{1}{\Delta A} = \frac{1}{\Delta A_0} + \frac{1}{2\varepsilon b}k_{bi}t \tag{4}$$

where ΔA_0 is the initial transient absorption signal at zero time delay. The second-order decay constant can then be extracted from the slope of a linear fit of the transient absorption data plotted as $1/\Delta A$ vs t according to

$$k_{bi} = 2\varepsilon b \times \text{slope} \tag{5}$$

The diffusion controlled triplet–triplet annihilation model has been used in the light emitting diode literature to examine diffusion lengths of triplets in organic crystalline materials.[7,32,33,44] In that work, the second-order decay constant k_{bi} could be related to the diffusion constant D of the triplets according to

$$k_{bi} = 8\pi R_C D \tag{6}$$

where R_C was the capture radius corresponding to the triplet–triplet encounter distance at which annihilation had unit probability.[47] Similar findings were obtained from studies of other bimolecular decay processes in which the second order rate constant was related to the diffusion constant of the mobile species and the reaction probability upon collisional encounter.[48–50] The diffusion constant in turn is related to the diffusion length l_D of the triplets according to

$$l_D = \sqrt{\tau D} \tag{7}$$

where τ again is the natural lifetime of the triplets that is determined by the intersystem crossing time needed for the excited molecule to change spin and return to the singlet ground state.

The first step toward using this model to characterize the triplet diffusion lengths in the nanocrystalline TIPS-Pn films was to measure the second-order decay constants for the triplet–triplet annihilation processes in the films. The triplet decay kinetics were plotted as $2\varepsilon b/\Delta A$ versus time on the nanosecond to 1.5 μs time scale in Figure 7b because the slopes of the data represent a direct measure of the second-order decay constants. Superimposed on the experimental data are linear fit functions from which the slopes of the $2\varepsilon b/\Delta A$ versus t plots were quantified. The linearity of the data demonstrates that the kinetics in each film were well-described by a second-order decay process with a single decay constant k_{bi} (see eq 4) even though the films annealed to varying extents consisted of nanoscale mixtures of amorphous, Form-II brickwork and 2D-brickwork phases of TIPS-Pn. It is interesting to note that the decay constants varied with changes of the phase composition of the TIPS-Pn films (the slopes of the $2\varepsilon b/\Delta A$ fit lines were unique to each film). The procedures by which the values of the extinction coefficients were obtained are summarized in Section S9, and their values for the $T_1 \rightarrow T_n$ transitions in the amorphous, Form-II brickwork and 2D brickwork films are tabulated in Table S2.

The slopes of the best fit lines through the $2\varepsilon b/\Delta A$ versus t data provided a direct measure of the second-order decay constants k_{bi} for each film. The second order decay constants are plotted on a logarithmic scale in Figure 7c versus the total mole fractions ϕ of the ordered phases of the corresponding

films. Because the second-order decay constants are proportional to the diffusion constants, our observation of more than a factor of 10 variation of the triplet diffusion constants between crystalline and amorphous systems is reminiscent of that for tetracene.[51] The error bars in Figure 7c are dominated by the uncertainties associated with the linear fits to the data in Figure 7b.

Because the partially solvent-annealed TIPS-Pn films contained nanoscale mixtures of three phases, we constructed a "Confined Triplet" kinetic model to describe the diffusion of triplet excitons among the phases. We assumed in this model that within the partially solvent-annealed films, triplet excitons were formed in each type of phase but did not exchange with triplet excitons formed in other phases.

Therefore, in the Confined Triplet kinetic model, we considered that the total population of triplet excitons in partially solvent-annealed TIPS-Pn films $[T]_{total}$ could be described by three populations of triplets that did not exchange: one in the disordered amorphous phase $[T]_{dis}$, one in the Form-II brickwork phase $[T]_{F2}$, and one in the 2D-brickwork phase $[T]_{2D}$

$$[T]_{total} = [T]_{dis} + [T]_{F2} + [T]_{2D} \tag{8}$$

Because the model was built on the assumption that triplet excitons did not exchange among the phases, we wrote three independent rate equations describing the time-evolution of these populations

$$\frac{d[T]_{dis}}{dt} = -\frac{1}{2}k_{dis}([T]_{dis})^2 \tag{9}$$

$$\frac{d[T]_{F2}}{dt} = -\frac{1}{2}k_{F2}([T]_{F2})^2 \tag{10}$$

$$\frac{d[T]_{2D}}{dt} = -\frac{1}{2}k_{2D}([T]_{2D})^2 \tag{11}$$

Solving the independent rate equations and substituting them into eq 8 yielded the time-dependence of the total triplet population

$$[T]_{total} = \frac{[T]_{0,dis}}{1 + \frac{1}{2}[T]_{0,dis}k_{dis}t} + \frac{[T]_{0,F2}}{1 + \frac{1}{2}[T]_{0,F2}k_{F2}t} + \frac{[T]_{0,2D}}{1 + \frac{1}{2}[T]_{0,2D}k_{2D}t} \tag{12}$$

where the $[T]_{0,x}$ is the initial triplet exciton population in phase x immediately following the pulsed excitation, and k_x is the second-order decay constant measured for phase x. Using the molar absorption coefficients determined for the triplet state absorption for each of the three phases (Table S2), the time-dependent absorption of the total triplet population could be determined.

We independently quantified all parameters in eq 12 ($[T]_{0,x}$ and k_x) using measurements of films consisting of the pure disordered, Form-II brickwork, and Type-II brickwork phases in order to calculate transient absorption kinetics predicted by the Confined Triplet kinetic model. The diffusion-controlled triplet–triplet annihilation kinetics of each phase were measured to determine the bimolecular rate constants (k_x) of the as-cast (amorphous), thermally annealed (Form-II brickwork) and fully solvent-annealed (2D-brickwork) films. Figure 8a depicts these transient absorption kinetics traces plotted as
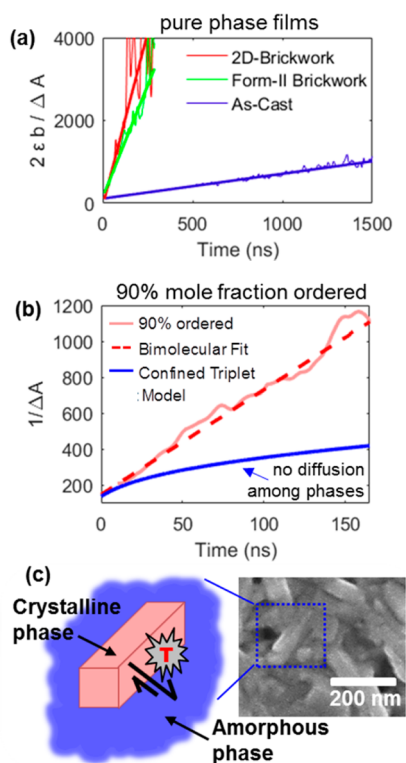
Figure 8. (a) Plot of $2\varepsilon b/\Delta A$ versus time measured in TIPS-Pn films consisting of pure phases. (b) Plot of $2\varepsilon b/\Delta A$ versus time measured in the partially solvent-annealed TIPS-Pn film with 90% mole fraction ordered phase. Overlaid on the data is a linear fit used to quantify the slope (dotted line). The solid curve represents triplet−triplet annihilation kinetics predicted from the Confined Triplet kinetic model in which triplet excitons cannot diffuse among the amorphous and ordered phases. (c) A conceptual cartoon describing the exchange of triplet excitons between both amorphous and crystalline phases.

$2\varepsilon b/\Delta A$ versus t that have been scaled to correct for differences among the molar absorption coefficients of their respective $T_1 \rightarrow T_n$ transitions for each film (Table S2). In order to calculate the initial triplet concentrations $[T]_{0,x}$ in each phase, knowledge of both the number of photons absorbed by each phase (concentration of singlet excitons) and the triplet quantum yields was required. We used the relative extinction coefficients of the $S_0 \rightarrow S_1$ transitions (see Figure 1b) along with the phase compositions of the partially annealed films to calculate the proportion of incident photons absorbed by the amorphous, Form-II brickwork, and 2D-brickwork phases. We then combined these values with the estimated triplet exciton quantum yields in each of the three phases (see Section S10) to calculate their initial triplet exciton concentrations. These corrections were again minor in comparison to the more than 1 order of magnitude variation of the second-order decay constants of the Form-II brickwork and 2D-brickwork phases versus the amorphous phase.

Figure 8b depicts a comparison of the triplet−triplet annihilation kinetics plotted as $2\varepsilon b/\Delta A$ versus t for the partially solvent-annealed TIPS-Pn film with 90% mole fraction ordered phase (Form-II brickwork +2D-brickwork) with the best fit line from a single bimolecular decay function used to quantify the slope. The data and fit line were reproduced from Figure 7b for comparison to the kinetics calculated from the Confined Triplet kinetic model (solid curve). Note the shorter time-axis in Figure 8b in comparison to Figure 8a. Because

triplets were assumed to not exchange among the phases in the kinetic model, the calculated kinetics were characterized by a fast decay of the triplet population due to annihilation in the ordered phases. After this fast annihilation process, the remaining triplets in the model resided exclusively in the amorphous phase with annihilation kinetics that were characterized by those measured in the amorphous (as-cast) TIPS-Pn film. It is evident that the Confined Triplet kinetic model does not describe the triplet−triplet annihilation process that actually occurs in the partially solvent-annealed TIPS-Pn film. Not only does the model predict the wrong slope of the $2\varepsilon b/\Delta A$ versus t plot, it also predicts a knee in the data due to cross over from fast triplet−triplet annihilation in the ordered phases to slower annihilation in the amorphous phase. This knee is not observed in the experimental data. As such, we find that the Confined Triplet kinetic model is unable to describe the triplet−triplet annihilation kinetics of any of the partially solvent-annealed films.

Inspection of the triplet−triplet annihilation kinetics in Figure 7b demonstrates that triplets undergo annihilation processes that reflect the average composition of the films rather than the kinetics of either the ordered or the amorphous phases. That this average between the ordered and amorphous phases varied quasi-continuously over a significant change of film composition and morphology indicated that triplet excitons were able to diffuse over distances sufficiently large that this average reflected the mole fractions of both amorphous and ordered domains. The cartoon in Figure 8c illustrates the dynamic exchange of triplet excitons that is implied by the smooth variation of the triplet−triplet annihilation kinetics with film composition. A magnified view of an SEM image of a TIPS-Pn film with 90% ordered content is included in the cartoon to show the approximate length scale over which triplet excitons must have diffused in order to exhibit annihilation kinetics that reflected the average composition of the film.

We considered the possibility that the second-order decay constants of the partially annealed films in Figure 7c might have increased smoothly with continued annealing due to a gradual increase of the intermolecular order among the TIPS-Pn molecules in the amorphous phase during the annealing process. However, the absorption spectra represented in Figure 1b and Figure 2a were very sensitive to the intermolecular interactions in the films (two very similar polymorphs have distinct absorption spectra). The sharp vibronic peaks of the amorphous phase did not appear to shift to longer wavelength but rather monotonically decreased in amplitude with continued annealing. Therefore, the data indicated that annealing caused a transfer of TIPS-Pn molecules from an amorphous to an ordered state (Form-II brickwork or 2D-brickwork) rather than a gradual increase of intermolecular interactions within the amorphous phase. We concluded therefore, that the variation of the second-order decay constants (Figure 7c) with continued annealing could not be explained in terms of an increase of intermolecular order within the amorphous phase during the annealing process. Again, it was necessary to include triplet exciton diffusion among the ordered and amorphous phases to describe the triplet−triplet annihilation kinetics measured in the TIPS-Pn films examined here.

Influence of an Amorphous Phase on Triplet Diffusion in TIPS-Pn Films. The smooth variation of the second-order decay constants between the limits of behavior defined by the

crystalline and amorphous phases in TIPS-Pn films (Figure 7c) indicated that triplet diffusion could be described as a single diffusion process in an averaged effective medium. Because the second-order decay constants are proportional to the diffusion constants (eq 6), the data indicate that triplet diffusion could be described by an effective diffusion constant that reflected the weighted average diffusion constant of the nanocrystalline TIPS-Pn films. Both the Scherrer analysis of the integrated 2D XRD measurements (Figure 5) and the SEM images of the TIPS-Pn films indicated that triplet excitons must diffuse over many tens of nanometers for the distribution of amorphous and crystalline phases to be well-described as an averaged effective medium.

We adopted the diffusion-mediated annihilation model[7,33,44] to estimate the triplet diffusion lengths predicted from the annihilation kinetics as a means to determine whether the kinetics are consistent with triplet diffusion over many tens of nanometers. eqs 6 and 7 demonstrate that the natural lifetime of triplet excitons τ and a capture radius R_C for triplet−triplet annihilation are needed to estimate the triplet diffusion lengths from the second-order decay constants (Figure 7c). We measured the natural lifetime of triplet excitons in TIPS-Pn films using the excitation density dependence of the transient absorption measurements of the triplet decay kinetics (see Sections S9 and S14). At the lowest excitation densities, a transition was observed from kinetics dominated by second-order triplet−triplet annihilation to a first order decay that was indicative of intersystem crossing. Triplet decay kinetics measured at the lowest excitation density of 6 μJ/cm^2 for the as-cast film are represented in Figure S24 and exhibited a clear exponential decay after 1 μs. We fit this exponential decay to quantify the natural lifetime $\tau = 2.1 \pm 0.3$ μs of triplet excitons in TIPS-Pn.

Having measured the natural lifetime, we discuss the capture radius R_C. Because we do not have an independent measure of the capture radius for triplet−triplet annihilation in TIPS-Pn films, we considered a range of values for R_C to estimate diffusion lengths. Figure 9a shows the variation of the estimated diffusion lengths versus the mole fraction of the amorphous phase $(1 − \phi$, where ϕ was defined above as the mole fraction of the ordered phases) in the partially solvent- annealed TIPS-Pn films. Diffusion lengths were calculated for three values of R_C: 0.4 nm, 0.7 and 1.4 nm. The smaller two values were motivated by consideration of the distances between neighboring TIPS-Pn molecules within the 2D-brickwork structure. A triplet−triplet capture radius of $R_C = 0.4$ nm is similar to the 0.41 nm spin confinement length recently reported in TIPS-Pn films on the basis of joint microwave susceptibility and light-induced electron spin resonance measurements.[52] This radius also corresponds to the closest distance of approach of the planes of the acene rings in the 2D-brickwork polymorph.[26,34,37,38] The triplet diffuson lengths calculated from the second-order decay constants for the set of partially solvent-annealed films varies from ∼14 to ∼75 nm as indicated in Figure 9a. For reference, the diffusion constants ranged from $(1.00 \pm 0.03) \times 10^{-6}$ cm^2/s to $(2.7 \pm 0.2) \times 10^{-5}$ cm^2/s. Tables listing the diffusion constants calculated for all the samples and for all the capture radii used here are provided in the Supporting Information (Tables S5−S7). Table S8, also in Supporting Information, contains the calculated diffusion lengths appearing in Figure 9a.

We also considered a capture radius of $R_C = 0.7$ nm because this distance corresponds to approximately half the core-to-core
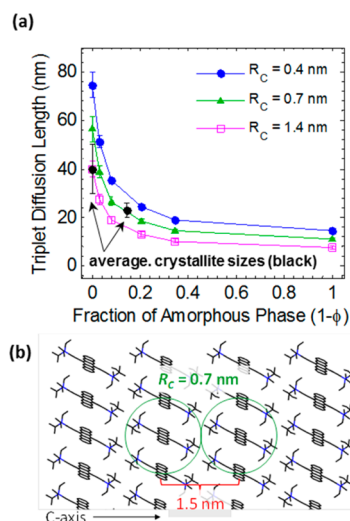

Figure 9. (a) Dependence of triplet diffusion length on mole fraction of the amorphous phase. Three triplet capture radii were considered: 0.4 nm, 0.7 and 3 nm as described in the text. Average crystallite sizes determined from 2D XRD measurements are included for reference. (b) The core-to-core intermolecular distance along the c-axis determined from the 2D-brickwork crystal structure is indicated to show the relevance of the $R_C = 0.7$ nm triplet capture radius.

spacing among the acene rings of TIPS-Pn molecules along the c-axis of the 2D-brickwork crystal (the direction separated by the triisopropylsilylethynyl side groups, Figure 9b). Adoption of an $R_C = 0.7$ nm means that two triplet excitons residing on neighboring molecules along the c-axis (being separated by $2R_C$) would have unit probability to annihilate. Along the other two crystal axes of the 2D-brickwork structure, this distance corresponds to two triplets on next-nearest neighbors having unit probability to annihilate. Figure 9a indicates that the range of triplet diffusion lengths calculated for this value of R_C varies from ∼11 to ∼56 nm.

It is reasonable to expect the triplet capture radius to depend on the precise molecular packing structure of TIPS-Pn. Therefore, we anticipate the radius will vary slightly for each sample presented here. For example, the 2D-brickwork and Form-II brickwork crystal polymorphs have been shown to have a difference in their average pi−pi stacking distance of ∼5%.[34] Additionally, the as-cast films consisting of disordered molecules may have even larger average intermolecular separation. Under the assumption that the film density does not significantly change between disordered and crystalline films, the largest intermolecular spacing in this case would roughly be the length of two triisopropylsilylethynyl side groups. This approximately corresponds to the crystallographic c vector, which gives a radius of ∼0.7 nm. Thus, we consider that the bounds of the capture radii considered above ($R_C = 0.4$ nm to $R_C = 0.7$ nm) encompass any possible variation of intermolecular distances occurring as a result of crystallization or polymorphism.

Finally, we calculated the capture radius that would be needed to predict triplet exciton diffusion lengths that matched the average crystallite sizes obtained from Scherrer analysis of the integrated 2D XRD measurements of the partially solvent-annealed films. This calculation was motivated by our intuition that triplet excitons might be confined within the crystallites in which they were originally formed. The average crystallite sizes of the fully solvent-annealed and the partially annealed film

with R_{700}/R_{648} = 0.7 (corresponding to ϕ = 90% ordered phases) are included in Figure 9a for comparison. We found it necessary to increase the value of the triplet capture radius R_C to 1.4 nm to make the calculated triplet exciton diffusion lengths match the average crystallite sizes present in the TIPS-Pn films.

Triplet capture radii of similar size have been reported in organic molecules such as rubrene[53] that undergo delayed fluorescence, or phosphorescent organic light emitting diode materials with heavy atoms like iridium.[33] In rubrene (and tetracene),[54,55] delayed fluorescence is observed because triplet fusion to reform the S_1 state upon collisional encounter of two T_1 states is exergonic. In fact, dynamic conversion between triplet pairs and singlet states has been observed in tetracene crystals[12,13] and gives rise to extended triplet transport distances in that system. Extended triplet capture radii can be observed in organic molecules such as rubrene because the triplet annihilation process may involve Forster-type triplet interactions.[56] The longer-range nature of Forster energy transfer would thus support a larger triplet capture radius.

However, in functionalized pentacenes singlet fission is exergonic,[46] which means that triplet fusion to reform a singlet exciton is endergonic (see energy diagram in Figure 1a). The energetically uphill process to reform the singlet state makes it more likely that triplets annihilate in TIPS-Pn by formation of a highly excited T_n state, which is a spin-conserved process.[57] However, such triplet states are unable to undergo Forster energy transfer because excited state triplet energy transfer to singlet ground state molecules involves a spin-forbidden de-excitation step.[45] We note that delayed fluorescence due to reformation of the S_1 state from triplet fusion has not been reported in TIPS-Pn, which is consistent with formation of a nonemissive T_n state during triplet–triplet annihilation. As such, the triplet capture radius in TIPS-Pn is expected to be much smaller because energy transfer would occur on smaller length scales as predicted from the Dexter mechanism. A smaller triplet capture radius is also consistent with the spin-confinement length for TIPS-Pn of 0.41 nm[52] that was recently reported, suggesting that triplet–triplet interactions are very local in TIPS-Pn. Consequently, we did not consider the ~27 nm triplet exciton diffusion length predicted from a value of R_C = 1.4 nm for the fully solvent-annealed TIPS-Pn film to be a physically sensible result. These considerations led us to conclude that triplet excitons have diffusion lengths between ~14 and ~75 nm in the series of partially solvent-annealed TIPS-Pn films as estimated from R_C values of 0.4 nm.

We were intrigued that the estimated ~75 nm triplet exciton diffusion length in the fully solvent-annealed TIPS-Pn film (fraction of amorphous phase = 0 in Figure 9a) was significantly larger than the ~40 nm average crysallite size calculated from Scherrer analysis of the 2D XRD measurements. This finding indicates that grain boundaries between TIPS-Pn crystallites do not necessarily impede triplet exciton diffusion, which is consistent with recent ultrafast microscopy measurements that suggest grain boundaries are not molecularly sharp.[18,26,58] The authors of that work showed that the interfaces of crystalline grain boundaries actually consist of molecules in the form of small nanocrystalline domains. Such interfaces may provide enough wave function overlap necessary for triplets to transfer across the boundaries, which is implied by the triplet–triplet annihilation behavior we observed.

These findings are consistent with the observation that triplet excitons experience an effective medium during their diffusion

that consists of a weighted average of the TIPS-Pn phases in the partially solvent-annealed films (see Figure 7). We suggest that triplet excitons were able to undergo dynamic exchange across grain boundaries between ordered and amorphous domains in the partially solvent-annealed films. Although triplet excitons in the ordered regions diffuse more rapidly than in the amorphous regions, as evidenced by their faster triplet–triplet annihilation kinetics, the dynamic exchange between the ordered and amorphous phases caused the diffusion of triplet excitons to be described by a single diffusion constant that is a weighted average of the constants corresponding to the two types of phases.

We note that our measurements of triplet exciton diffusion constants in the as-cast and fully solvent-annealed films permit us to consider the partitioning of triplets among these phases as they undergo dynamic exchange. Considering equal populations of triplet excitons generated near the phase boundaries, we estimate using Fick's law that the initial flux of triplets diffusing into the amorphous phase from the crystalline phase would be ~27 times larger than the opposite direction because of the differences in diffusivity of the phases. Considering that under one-sun irradiation conditions bimolecular recombination of triplet excitons is a negligible decay pathway[7] for pentacene films, we conclude that the lifetime of triplet excitons in the amorphous phase would not be limited by concentration-dependent annihilation. Net transfer of triplet excitons from the crystalline to the amorphous phases would occur until the population in the amorphous phases increases sufficiently to balance the flux in the opposite direction. If we assume the probability of triplet transfer across the interface in either direction is unity, then for an initially equal concentration of triplet excitons in both amorphous and crystalline phases, approximately 97% of the original triplet population would end up in the amorphous phase.

This net transfer of triplet population into the amorphous phase explains why the presence of even a small amount of amorphous material has such a large impact on the diffusion length of triplet excitons (Figure 9a). This conclusion is valid regardless of the value of R_C that is assumed in the diffusion length calculation. This finding may have significant implications for current efforts targeting new singlet fission sensitizers,[39] especially those based on polymeric systems.[19–22]

For example, even the most highly ordered polymers such as polyethylene contain significant fractions of an amorphous component.[59] It may be necessary to target polymer-based singlet fission sensitizers that, like poly(3-hexylthiophene),[60] undergo marked changes of their electronic energy levels upon crystallization.[18] We note that TIPS-Pn exhibits some degree of energetic change of the S_1 state with crystallization (Figure 1b). However, because triplet excitons are more localized than their singlet counterparts, the energetic step going from crystalline to amorphous phases is not sufficient to confine triplet excitons in the case of TIPS-Pn. We therefore conclude that singlet fission sensitizers with even greater singlet and triplet excitonic energy differences between crystalline and amorphous phases may be necessary to confine triplets to the crystalline phases of polymer films, thereby maintaining high triplet exciton diffusivity in spite of the potential presence of amorphous domains.

■ CONCLUSIONS

We demonstrated a new spin-casting and solvent annealing method to vary the intermolecular order and morphology of thin films of TIPS-Pn, a model singlet fission chromophore.

TIPS-Pn films spin-cast from dichloromethane were amorphous with absorption spectra that closely resembled the corresponding absorption spectra in solution, indicating weak electronic interactions between molecules. Gentle solvent annealing with 2-propanol, a poor solvent for TIPS-Pn, enabled us to systematically tune and arrest the evolution of the intermolecular order and morphology of the films.

By controlling the crystallization of TIPS-Pn, we investigated how the rates of singlet fission versus triplet–triplet annihilation depended on molecular packing using a combination of transient absorption spectroscopy and quantitative thin film characterization. The second-order decay constants describing triplet–triplet annihilation kinetics varied by nearly 2 orders of magnitude in TIPS-Pn films spanning a range of morphologies from amorphous to a completely crystalline 2D-brickwork. Within this range, films were found to consist of nanoscale mixtures comprising both amorphous and crystalline phases.

The annihilation kinetics of triplet excitons formed by singlet fission were well-described by single second-order rate constants even in films that consisted of nanoscale mixtures of crystalline and amorphous phases. Furthermore, the second-order rate constants varied smoothly with changes of film morphology, indicating that triplets undergo dynamic exchange across phase boundaries between the crystalline and amorphous phases. By adopting a diffusion model[33] describing triplets that undergo annihilation, we determined that the triplet diffusion lengths varied from ∼14 to ∼75 nm depending on the mole fraction of amorphous phase in the films. Overall, our findings suggest that controlling intermolecular packing among singlet fission chromophores is critical for maximizing triplet exciton diffusion lengths, which can be attenuated significantly by the presence of even small amounts of an amorphous phase. This finding also suggests that ongoing efforts to identify new singlet fission sensitizers based on polymeric materials should target polymers that undergo marked changes in their electronic energy levels when they crystallize. In such semicrystalline systems, large energy differences between amorphous and crystalline phases may pose a barrier to triplet exchange between them. This design would effectively confine triplet excitons to their crystalline regions, thereby avoiding the reduction of their diffusivity despite the presence of amorphous domains.

ASSOCIATED CONTENT

Ⓢ Supporting Information

The Supporting Information is available free of charge on the ACS Publications website at DOI: 10.1021/jacs.6b10010.

> Detailed experimental methods, analysis of absorption spectra and X-ray diffraction patterns, thermal annealing procedures, calculation of triplet absorption cross sections and yields, kinetic modeling, and SEM imaging (PDF)

AUTHOR INFORMATION

Corresponding Authors
*anthony@uky.edu
*jasbury@psu.edu

ORCID Ⓘ

Gregory D. Scholes: 0000-0003-3336-7960
John E. Anthony: 0000-0002-8972-1888
John B. Asbury: 0000-0002-3641-7276

REFERENCES

(1) Smith, M. B.; Michl, J. *Chem. Rev.* **2010**, *110*, 6891−6936.
(2) Shockley, W.; Queisser, H. J. *J. Appl. Phys.* **1961**, *32*, 510−519.
(3) Walker, B. J.; Musser, A. J.; Beljonne, D.; Friend, R. H. *Nat. Chem.* **2013**, *5*, 1019−24.
(4) Sanders, S. N.; Kumarasamy, E.; Pun, A. B.; Trinh, M. T.; Choi, B.; Xia, J.; Taffet, E. J.; Low, J. Z.; Miller, J. R.; Roy, X.; Zhu, X. Y.; Steigerwald, M. L.; Sfeir, M. Y.; Campos, L. M. *J. Am. Chem. Soc.* **2015**, *137*, 8965−8972.
(5) Tabachnyk, M.; Ehrler, B.; Bayliss, S.; Friend, R. H.; Greenham, N. C. *Appl. Phys. Lett.* **2013**, *103*, 153302.
(6) Reusswig, P. D.; Congreve, D. N.; Thompson, N. J.; Baldo, M. A. *Appl. Phys. Lett.* **2012**, *101*, 113304.
(7) Poletayev, A. D.; Clark, J.; Wilson, M. W.; Rao, A.; Makino, Y.; Hotta, S.; Friend, R. H. *Adv. Mater.* **2014**, *26*, 919−924.
(8) Yang, L.; Tabachnyk, M.; Bayliss, S. L.; Bohm, M. L.; Broch, K.; Greenham, N. C.; Friend, R. H.; Ehrler, B. *Nano Lett.* **2015**, *15*, 354−358.
(9) Piland, G. B.; Burdett, J. J.; Dillon, R. J.; Bardeen, C. J. *J. Phys. Chem. Lett.* **2014**, *5*, 2312−2319.
(10) Najafov, H.; Lee, B.; Zhou, Q.; Feldman, L. C.; Podzorov, V. *Nat. Mater.* **2010**, *9*, 938−943.
(11) Akselrod, G. M.; Deotare, P. B.; Thompson, N. J.; Lee, J.; Tisdale, W. A.; Baldo, M. A.; Menon, V. M.; Bulovic. *Nat. Commun.* **2014**, *5*, 3646.
(12) Wan, Y.; Guo, Z.; Zhu, T.; Yan, S.; Johnson, J.; Huang, L. *Nat. Chem.* **2015**, *7*, 785−792.
(13) Zhu, T.; Wan, Y.; Guo, Z.; Johnson, J.; Huang, L. *Adv. Mater.* **2016**, *28*, 7539−7547.
(14) Kawata, S.; Pu, Y. J.; Saito, A.; Kurashige, Y.; Beppu, T.; Katagiri, H.; Hada, M.; Kido, J. *Adv. Mater.* **2016**, *28*, 1585−1590.
(15) Margulies, E. A.; Wu, Y.-L.; Gawel, P.; Miller, S. A.; Shoer, L. E.; Schaller, R. D.; Diederich, F.; Wasielewski. *Angew. Chem., Int. Ed.* **2015**, *54*, 8679−8683.
(16) Elfers, N.; Lyskov, I.; Spiegel, J. D.; Marian, C. M. *J. Phys. Chem. C* **2016**, *120*, 13901−13910.
(17) Chien, A. D.; Molina, A. R.; Abeyasinghe, N.; Varnavski, O. P.; Goodson, T.; Zimmerman, P. M. *J. Phys. Chem. C* **2015**, *119*, 28258−28268.
(18) Wong, C. Y.; Folie, B. D.; Cotts, B. L.; Ginsberg, N. S. *J. Phys. Chem. Lett.* **2015**, *6*, 3155−3162.
(19) Busby, E.; Xia, J.; Wu, Q.; Low, J. Z.; Song, R.; Miller, J. R.; Zhu, X. Y.; Campos, L. M.; Sfeir, M. Y. *Nat. Mater.* **2015**, *14*, 426−433.
(20) Kasai, Y.; Tamai, Y.; Ohkita, H.; Benten, H.; Ito, S. *J. Am. Chem. Soc.* **2015**, *137*, 15980−15983.
(21) Musser, A. J.; Al-Hashimi, M.; Maiuri, M.; Brida, D.; Heeney, M.; Cerullo, G.; Friend, R. H.; Clark, J. *J. Am. Chem. Soc.* **2013**, *135*, 12747−12754.
(22) Zhai, Y.; Sheng, C.; Vardeny, Z. V. *Philos. Trans. R. Soc., A* **2015**, *373*, 20140327.
(23) Roberts, S. T.; McAnally, R. E.; Mastron, J. N.; Webber, D. H.; Whited, M. T.; Brutchey, R. L.; Thompson, M. E.; Bradforth, S. E. *J. Am. Chem. Soc.* **2012**, *134*, 6388−6400.

(24) Arias, D. H.; Ryerson, J. L.; Cook, J. D.; Damrauer, N. H.; Johnson, J. C. *Chem. Sci.* **2016**, *7*, 1185−1191.

(25) Hartnett, P. E.; Margulies, E. A.; Mauck, C. M.; Miller, S. A.; Wu, Y.; Wu, Y. L.; Marks, T. J.; Wasielewski, M. R. *J. Phys. Chem. B* **2016**, *120*, 1357−1366.

(26) Sharifzadeh, S.; Wong, C. Y.; Wu, H.; Cotts, B. L.; Kronik, L.; Ginsberg, N. S.; Neaton, J. B. *Adv. Funct. Mater.* **2015**, *25*, 2038−2046.

(27) Yost, S. R.; Lee, J.; Wilson, M. W.; Wu, T.; McMahon, D. P.; Parkhurst, R. R.; Thompson, N. J.; Congreve, D. N.; Rao, A.; Johnson, K.; Sfeir, M. Y.; Bawendi, M. G.; Swager, T. M.; Friend, R. H.; Baldo, M. A.; Van Voorhis, T. *Nat. Chem.* **2014**, *6*, 492−497.

(28) Dillon, R. J.; Piland, G. B.; Bardeen, C. J. *J. Am. Chem. Soc.* **2013**, *135*, 17278−17281.

(29) Pensack, R. D.; Tilley, A. J.; Parkin, S. R.; Lee, T. S.; Payne, M. M.; Gao, D.; Jahnke, A. A.; Oblinsky, D. G.; Li, P. F.; Anthony, J. E.; Seferos, D. S.; Scholes, G. D. *J. Am. Chem. Soc.* **2015**, *137*, 6790−6803.

(30) Wu, Y.; Liu, K.; Liu, H.; Zhang, Y.; Zhang, H.; Yao, J.; Fu, H. *J. Phys. Chem. Lett.* **2014**, *5*, 3451−3455.

(31) Herz, J.; Buckup, T.; Paulus, F.; Engelhart, J.; Bunz, U. H.; Motzkus, M. *J. Phys. Chem. Lett.* **2014**, *5*, 2425−2430.

(32) Lin, J. D. A.; Mikhnenko, O. V.; Chen, J.; Masri, Z.; Ruseckas, A.; Mikhailovsky, A.; Raab, R. P.; Liu, J.; Blom, P. W. M.; Loi, M. A.; García-Cervera, C. J.; Samuel, I. D. W.; Nguyen, T.-Q. *Mater. Horiz.* **2014**, *1*, 280−285.

(33) Zhang, Y.; Forrest, S. R. *Chem. Phys. Lett.* **2013**, *590*, 106−110.

(34) Diao, Y.; Lenn, K. M.; Lee, W. Y.; Blood-Forsythe, M. A.; Xu, J.; Mao, Y.; Kim, Y.; Reinspach, J. A.; Park, S.; Aspuru-Guzik, A.; Xue, G.; Clancy, P.; Bao, Z.; Mannsfeld, S. C. *J. Am. Chem. Soc.* **2014**, *136*, 17046−17057.

(35) Giri, G.; Li, R.; Smilgies, D. M.; Li, E. Q.; Diao, Y.; Lenn, K. M.; Chiu, M.; Lin, D. W.; Allen, R.; Reinspach, J.; Mannsfeld, S. C.; Thoroddsen, S. T.; Clancy, P.; Bao, Z.; Amassian, A. *Nat. Commun.* **2014**, *5*, 3573.

(36) Giri, G.; Verploegen, E.; Mannsfeld, S. C.; Atahan-Evrenk, S.; Kim do, H.; Lee, S. Y.; Becerril, H. A.; Aspuru-Guzik, A.; Toney, M. F.; Bao, Z. *Nature* **2011**, *480*, 504−508.

(37) Anthony, J. E.; Brooks, J. S.; Eaton, D. L.; Parkin, S. R. *J. Am. Chem. Soc.* **2001**, *123*, 9482−9483.

(38) James, D. T.; Frost, J. M.; Wade, J.; Nelson, J.; Kim, J. *ACS Nano* **2013**, *7*, 7983−7991.

(39) Lloyd, M. T.; Mayer, A. C.; Tayi, A. S.; Bowen, A. M.; Kasen, T. G.; Herman, D. J.; Mourey, D. A.; Anthony, J. E.; Malliaras, G. G. *Org. Electron.* **2006**, *7*, 243−248.

(40) Matsubara, R.; Sakai, M.; Kudo, K.; Yoshimoto, N.; Hirosawa, I.; Nakamura, M. *Org. Electron.* **2011**, *12*, 195−201.

(41) Smith, M. B.; Michl, J. *Annu. Rev. Phys. Chem.* **2013**, *64*, 361−386.

(42) Ramanan, C.; Smeigh, A. L.; Anthony, J. E.; Marks, T. J.; Wasielewski, M. R. *J. Am. Chem. Soc.* **2012**, *134*, 386−397.

(43) Pensack, R. D.; Ostroumov, E. E.; Tilley, A. J.; Mazza, S.; Grieco, C.; Thorley, K. J.; Asbury, J. B.; Seferos, D. S.; Anthony, J. E.; Scholes, G. D. *J. Phys. Chem. Lett.* **2016**, *7*, 2370−2375.

(44) Baldo, M. A. A. C.; Forrest, S. R. *Phys. Rev. B: Condens. Matter Mater. Phys.* **2000**, *62*, 10967−10977.

(45) Mirkovic, T.; Ostroumov, E. E.; Anna, J. M.; van Grondelle, R.; Govindjee; Scholes, G. D. *Chem. Rev.* **2016**, DOI: 10.1021/acs.chemrev.6b00002.

(46) Zhang, Y. D.; Wu, Y.; Xu, Y.; Wang, Q.; Liu, K.; Chen, J. W.; Cao, J. J.; Zhang, C.; Fu, H.; Zhang, H. L. *J. Am. Chem. Soc.* **2016**, *138*, 6739−6745.

(47) Chandrasekhar, S. *Rev. Mod. Phys.* **1943**, *15*, 1−89.

(48) Noolandi, J.; Hong, K. M. *J. Chem. Phys.* **1979**, *70*, 3230−3236.

(49) Samoc, M.; Williams, D. F. *J. Chem. Phys.* **1983**, *78*, 1924−1930.

(50) Braun, C. L. *J. Chem. Phys.* **1984**, *80*, 4157−4161.

(51) Yost, S. R.; Hontz, E.; Yeganeh, S.; Van Voorhis, T. *J. Phys. Chem. C* **2012**, *116*, 17369−17377.

(52) Bayliss, S. L.; Thorley, K. J.; Anthony, J. E.; Bouchiat, H.; Greenham, N. C.; Chepelianskii, A. D. *Phys. Rev. B: Condens. Matter Mater. Phys.* **2015**, *92*, 115432.

(53) Jia, W.; Chen, Q.; Chen, L.; Yuan, D.; Xiang, J.; Chen, Y.; Xiong, Z. *J. Phys. Chem. C* **2016**, *120*, 8380−8386.

(54) Tomkiewicz, Y.; Groff, R. P.; Avakian, P. *J. Chem. Phys.* **1971**, *54*, 4504−4507.

(55) Groff, R. P.; Avakian, P.; Merrifield, R. E. *Phys. Rev. B* **1970**, *1*, 815−817.

(56) van Eersel, H.; Bobbert, P. A.; Coehoorn, R. *J. Appl. Phys.* **2015**, *117*, 115502.

(57) Saltiel, J.; Marchand, G. R.; Smothers, W. K.; Stout, S. A.; Charlton, J. L. *J. Am. Chem. Soc.* **1981**, *103*, 7159−7164.

(58) Wong, C. Y.; Cotts, B. L.; Wu, H.; Ginsberg, N. S. *Nat. Commun.* **2015**, *6*, 5946.

(59) Richardson, M. J. *Br. Polym. J.* **1969**, *1*, 132−137.

(60) Tsoi, W. C.; Spencer, S. J.; Yang, L.; Ballantyne, A. M.; Nicholson, P. G.; Turnbull, A.; Shard, A. G.; Murphy, C. E.; Bradley, D. D. C.; Nelson, J.; Kim, J.-S. *Macromolecules* **2011**, *44*, 2944−2952.